Permittivity Threshold and Thermodynamics of Integer Charge-Transfer Complexation for an Organic Donor-Acceptor Pair

Brandon J. Barrett†, Howard E. Katz‡, and Arthur E. Bragg†*
†Department of Chemistry, Johns Hopkins University, 3400 N. Charles St., Baltimore, MD 21218, U.S.A.
‡Department of Material Science & Engineering, Johns Hopkins University, 3400 N. Charles St., Baltimore, MD 21218, U.S.A.

Abstract. Molecular charge doping involves the formation of donor-acceptor charge-transfer complexes (CTCs) through integer or partial electron transfer; understanding how local chemical environment impacts complexation is important for controlling the properties of organic materials. We present steady-state and temperature-dependent spectroscopic investigations of the p-dopant 2,3,5,6-tetrafluoro-7,7,8,8-tetracyanoquinodimethane (F_4TCNQ) complexed with the electron donor and hole transport material *N,N'*-Diphenyl-*N*-*N'*-di-p-tolylbenzene-1,4-diamine (MPDA). Equilibrium formation constants (K_{CT}) were determined for donor-acceptor pairs dissolved in a series of solvents covering a range of values of permittivity. A threshold for highly favorable complex formation was observed to occur at ϵ~8-9, with large (>10^4) and small (<10^3) values of K_{CT} obtained in solvents of higher and lower permittivity, respectively, but with chloroform (ϵ=4.81) exhibiting an anomalously high formation constant. Temperature-dependent formation constants were determined in order to evaluate the thermodynamics of complex formation. In 1,2-dichloroethane (ϵ=10.36) and chlorobenzene (ϵ=5.62), complex formation is both enthalpically and entropically favorable, with higher enthalpic and entropic stabilization in the solvent with higher permittivity. Complexation in chloroform is exothermic and entropically disfavored, indicating that specific, inner-shell solvent-solute interactions stabilize the charge-separated complex and result in a net increase in local solution structure. Our results provide insight on how modification to the chemical environment may be utilized to support stable integer charge transfer for molecular doping applications and requiring only modest changes in local permittivity.

TOC Graphic

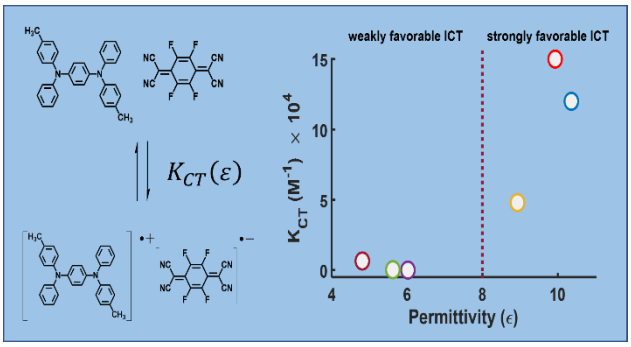
$K_{CT}(\varepsilon)$
weakly favorable ICT
strongly favorable ICT
K_{CT} (M^{-1}) × 10^4
15
10
5
0
4
6
8
10
Permittivity (ϵ)

Introduction

Molecular charge donor-acceptor interactions have recently attracted attention for charge-carrier doping in organic semiconducting materials.[1-4] Paired donors and acceptors support ground-state charge-transfer complexes (CTCs),[5] which have distinct electronic and spectroscopic properties: in accordance with Mulliken theory, the highest occupied molecular orbital (HOMO) of the donor and the lowest occupied molecular orbital (LUMO) of the acceptor mix, shifting the dopant energy levels and creating new absorption features that are sensitive to the donor ionization energy and acceptor electron affinity.[6-7] If the acceptor's LUMO level is sufficiently low relative to the donor's HOMO, spontaneous integer ground-state charge transfer from donor to acceptor occurs.[8-9] Integer charge transfer (ICT) has been used to p-dope organic semiconductors with radical cation polarons,[10-13] yet even partial charge transfer (PCT) arising from mixing of donor and acceptor energy levels has been used to improve charge transport in organic materials.[13] In this work we consider specifically the impacts of chemical environment on ICT relevant for molecular doping.

Quinone-based acceptors with large electron affinities, including 7,7,8,8-tetracyanoquinodimethane (TCNQ) and 2,3,5,6-tetrafluoro-7,7,8,8-tetracyanoquinodimethane (F_4TCNQ, Chart 1), are commercially-available and have been used extensively as molecular p-dopants.[12-15] Given the significant increase in the electron affinity of TCNQ with fluorination,[8] integer CTC formation with F_4TCNQ is possible for a broad range of electron donors, including polythiophenes (PT), tetrathiafulvavene (TTF), and phenylene diamines. A clear spectroscopic signature of (integer) donor-to-F_4TCNQ electron transfer is the structured near-infrared (NIR) absorption band of the F_NTCNQ radical anion.[8, 16-17] The frequencies of cyano (CN) stretching

vibrations, which are highly sensitive to local electric field, are also valuable reporters for the degree of charge separation between donors and the F_4TCNQ acceptor.[16, 18-20]

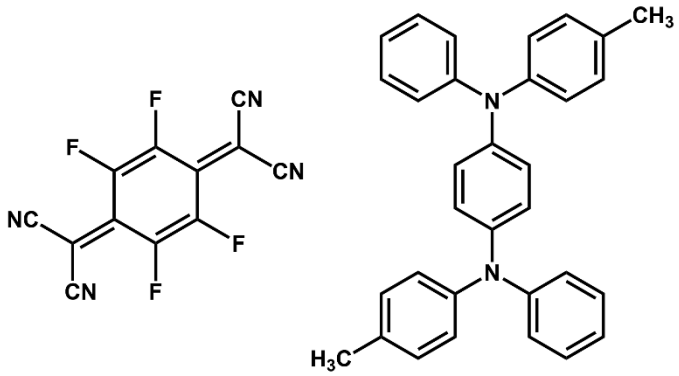

Chart 1. Electron acceptor 2,3,5,6-tetrafluoro-7,7,8,8-tetracyanoquinodimethane (F_4TCNQ, left) and donor *N,N'*-Diphenyl-*N*-*N'*-di-p-tolyl benzene-1,4-diamine (MPDA, right).

F_4TCNQ and other electron acceptors have been used extensively to p-dope conjugated organics (such as poly(3-hexylthiophene-2,5-diyl) (P3HT)) to increase charge-carrier densities.[20-21] Interestingly, both integer and partial charge transfer has been observed in film blends of P3HT with F_4TCNQ. Studies have shown that an ICT state is formed as the kinetically favored product during film processing but converts to the more thermodynamically favored PCT state.[20] There have been various efforts to control ICT vs PCT doping in organic films, as well as the degree of charge transfer, to improve charge mobility.[10, 21-25] For example, acceptor strength has been used to control the degree of charge transfer in film blends of pentacene with F_4TCNQ or 2,2′-(perfluoronaphthalene-2,6-diylidene)dimalononitrile (F_6TCNNQ): F_4TCNQ has a lower electron affinity and exhibits both ICT and PCT, the extent of which is controlled by mixing ratio; by contrast, F_6TCNNQ has a higher electron affinity and results only in ICT (but at the cost of a much less stable dopant species).[22] Relatedly, mobile polarons in P3HT have been generated by doping with large borane clusters exhibiting high electron affinities; increased mobility results from the greater charge-pair separation facilitated by microstructures incorporating the larger dopant

structure.[11] Integer charge transfer is favored by increasing the thermodynamic driving force for charge separation by increasing polaron stability, which is observed in ordered vs. disordered regions of polythiophenes, wherein the interconnection between electronic structure and polymer microstructure influences the density of states for ICT vs PCT.[21] It has also been shown that increasing the doping ratio of F_4TCNQ in films of poly[bis(4-phenyl)(2,4,6-trimethylphenyl)amine] (PTAA), a hole transport material,[26-27] leads to the growth of J-aggregates that support ICT; however excessive doping can lead to a conversion to PCT states in hole transport layers for organic light emitting diodes.[23]

Although the favorability of ICT is highly dependent on the relationship between acceptor EA and donor IP and may also be sensitive to material microstructure, the results described above do not consider how the relative stabilities of integer CTCs depend on local environment, particularly in materials that are generally characterized by low permittivity and polarity. Under these conditions, the stability of complexes may be limited by the non- or weakly polar surrounding material environment. For example, we previously observed an evolution between ICT and PCT states for CTCs of F_4TCNQ with *N,N'*-Diphenyl-*N*-*N'*-di-p-tolyl benzene-1,4-diamine (MPDA, Chart 1) doped in drop-cast films of polystyrene during the course of film processing, which is attributed to reduced stability of a solvent-stabilized integer CTC as the film dries.[16]

With an interest in understanding further the limits for controlling the stability of ICT states in films and devices, here we examine the role of the surrounding medium. We focused on complexation between F_4TCNQ and MPDA, where the latter is related to hole-transporting materials used in OLED architectures.[28-33] Notably, the ionization energy (IE) of MPDA is 5.5 eV,[29] which is comparable to that of oligo- and poly- thiophenes (e.g. quaterthiophene (4T), IE = 5.3 eV).[13] In order to assess the dependence on local medium, we determined the formation

constant, K_{CT}, for $MPDA^{\cdot+}$:$F_4TCNQ^{\cdot-}$ charge-transfer complexes in a series of weakly to moderately polar solvents characterized by a range in permittivity. Furthermore, we conducted temperature-dependent spectroscopic studies to determine enthalpies and entropies of CTC formation to compare cases of strongly vs. weakly favorable charge separation and assess interactions underlying stability of complexes. Our findings highlight the role the local environment has for maintaining fully charge-separated pairs and reveal that only modest changes in permittivity are needed to preparing organic material environments that favor integer charge-transfer complex formation.

Methods

*Sample Preparation***.** Dichloroethane (DCE), 1,2-Dichlorobenzene (oDCB), Dichloromethane (DCM), Chlorobenzene (CB), and Chloroform ($CHCl_3$) were purchased from Fischer Scientific and used without further purification. *N,N'*-Diphenyl-*N,N'*-di-p-tolyl benzene-1,4-diamine (MPDA) was purchased from Sigma-Aldrich and used as received. F_4TCNQ was purchased from BOC Sciences (97% purity) and used as received.

Solution samples of integer charge-transfer complexes were prepared from stock solutions of F_4TCNQ and MPDA for steady-state UV-Vis characterization; solutions were prepared using calibrated micropipettes for additions of each solution and solvent. F_4TCNQ stock solutions were prepared at concentrations near 10^{-5} M; MPDA stock solutions were prepared at concentrations between 10^{-4} and 10^{-3} M. CTC solutions were prepared at a constant acceptor concentration but with various donor concentrations by combining 1-2 mL of F_4TCNQ stock with 100 – 850 μL of MPDA stock solution and diluting with solvent to a total solution volume between 3-5 mL. On average 15 solutions (at various donor concentrations) were prepared for a given solvent.

Spectroscopic Characterizations. Room temperature UV-Vis spectra were collected with a diode array spectrometer that is fiber-optically coupled to tungsten and deuterium lamps (Stellarnet). Temperature-dependent UV-Vis spectra were collected using a Unisoku UnispeKs CoolSpeK UV USP-203 series cryostat. The fiber optics coupled to our light source(s) and spectrograph were mounted on either side of the sample chamber and aligned for optimized collection of transmitted light. A light flow of dry air from a purge generator was introduced into the sample chamber to prevent condensation or window fogging. For temperature-dependent measurements, samples were allowed to equilibrate thermally within the cryostat for 4-5 minutes before collecting spectra.

*Computations***.** Free energies for donor oxidation and acceptor reduction were computed at the DFT-level using the Johns Hopkins Rockfish Cluster and the Orca 4.2.0 software suite.[34-35] All structure optimizations applied the M06-L functional with the Ahlrichs basis sets,[36-37] def2-SVP applied to C and H and def2-TZVPP applied to all other atoms, and the def2/J auxiliary basis set.[38] Solvent effects were modeled using the conductor-like polarizable continuum model (cpcm) with dielectric constants appropriate for each solvent system considered. Vibrational frequency calculations were performed to confirm numerical precision and calculate the enthalpic and entropic contributions to free energy changes.

Results and Discussion

*Permittivity-Dependent Formation of $MPDA^{\cdot+}$:$F_4TCNQ^{\cdot-}$ Charge Transfer Complexes in Solution***.** UV/Vis absorption spectra of MPDA, F_4TCNQ and their CTC ($MPDA^{\cdot+}$:$F_4TCNQ^{\cdot-}$) dissolved in dichloroethane (DCE) are presented in Figure 1a. The CTC is formed spontaneously in DCE and exhibits absorption features in both the NIR (650-1100 nm) and near-UV (400 nm)

regions of the spectrum. Absorption spectra collected for $F_4TCNQ^{\cdot-}$ and $MPDA^{\cdot+}$ isolated through the constant potential electrolysis (CPE) of $MPDA^{\cdot+}$:$F_4TCNQ^{\cdot-}$ in DCE are plotted in Figure 1b.[16] The vibronic structure observed in the NIR for the CTC is characteristic of the radical anion's $D_0 \rightarrow D_1$ electronic transition. The MPDA radical cation has a broad, featureless absorption band spanning 600-1100 nm that overlaps with the sharp spectral features of the reduced acceptor.[16] The spectrum of the CTC appears to be a combination of overlapping $MPDA^{\cdot+}$ and $F_4TCNQ^{\cdot-}$ absorption features. We employed the method of continuous variation (or Job's analysis) to confirm the stoichiometry of complexes.[39] Absorption spectra collected at a constant total donor+acceptor concentration (~$6x10^{-5}$ M) but at different donor:acceptor mole fractions are presented in Figure S1; the absorbance at 865 nm is plotted vs. MPDA mole fraction in Figure S2 (a so-called Job's plot[40-41]). The CTC absorption peaks at 0.5 MPDA mole fraction, confirming that the $MPDA^{\cdot+}$:$F_4TCNQ^{\cdot-}$ CTC has a 1:1 donor: acceptor stoichiometry.

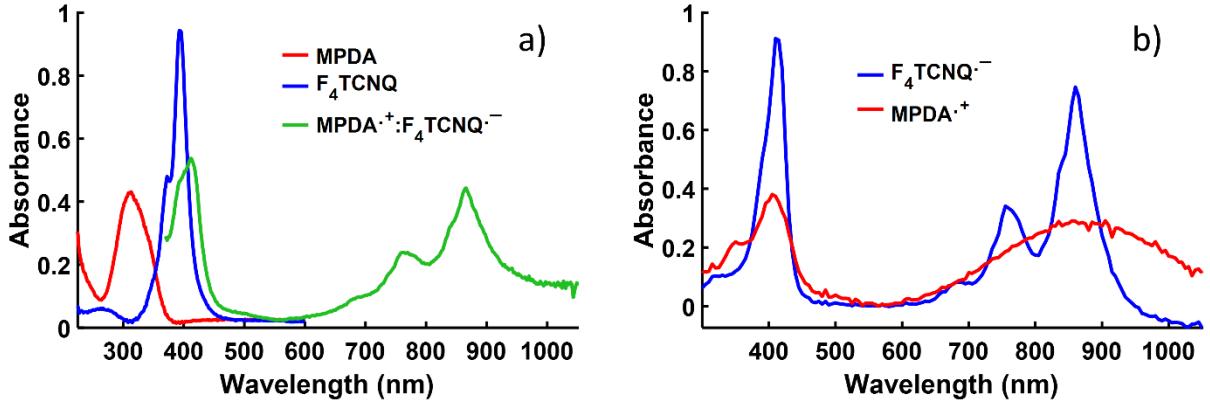

Figure 1. (a) UV-Vis absorption spectra of MPDA (red), F_4TCNQ (blue), and the $MPDA^{\cdot+}$:$F_4TCNQ^{\cdot-}$ integer charge-transfer complex (green) in dichloroethane (DCE) solution. (b) UV-Vis absorption spectra of $F_4TCNQ^{\cdot-}$ (blue) and $MPDA^{\cdot+}$ (red) generated electrochemically by constant potential electrolysis (CPE) of a solution of $MPDA^{\cdot+}$:$F_4TCNQ^{\cdot-}$ in DCE. CPE was conducted with 0.091 mM MPDA with excess F_4TCNQ and 0.12 mM F_4TCNQ with excess MPDA for 10 min at 0.410 and -0.090 V vs. Fc/Fc^+, respectively, both of which result in neutralizing the corresponding anion or cation species, respectively. Further details can be found in Reference 16.

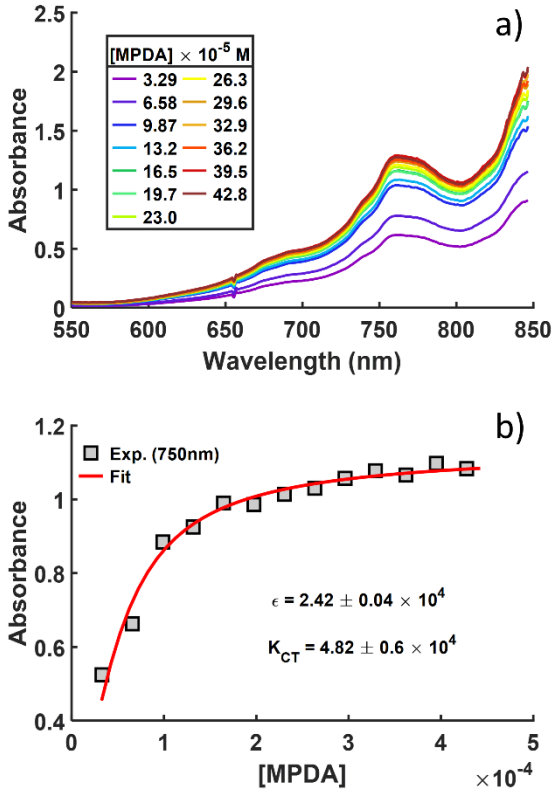

Figure 2. (a) UV-Vis absorption spectra collected with solutions of $MPDA^{\cdot+}$:$F_4TCNQ^{\cdot-}$ charge-transfer complexes dissolved in dichloromethane (DCM) prepared at various MPDA concentrations ($[F_4TCNQ] = 4.71\times10^{-5}$ M). (b) Absorbance of $MPDA^{\cdot+}$:$F_4TCNQ^{\cdot-}$ complexes in DCM at 750 nm as a function of the initial donor concentration (squares). The fit to the nonlinear model expressed in Equation 2 is overlaid (red solid line). Measurements were conducted at 21 ºC.

UV-Vis spectra were collected with CTC solutions prepared with a fixed F_4TCNQ concentration and a broad range of MPDA concentrations in order to determine equilibrium constants for charge-transfer complexation, K_{CT}. Figure 2a plots a series of absorption spectra collected with $MPDA^{\cdot+}$:$F_4TCNQ^{\cdot-}$ CTC solutions in dichloromethane (DCM) prepared with different MPDA concentrations. All spectra exhibit the characteristic absorption features of the F_4TCNQ radical anion in the near IR. The optical density at 750 nm is plotted as symbols (squares) in Figure 2b as a function of donor concentration for this series. The absorbance increases with

donor concentration with saturation. The donor and acceptor concentrations used to prepare each solution and corresponding CTC absorbance/optical density at 750 nm are listed in Table S1.

The complexation equilibrium is captured by Equation 1:

$$K_{CT} = \frac{C_{AD}}{(C_A^0 - C_{AD})(C_D^0 - C_{AD})} \quad (1)$$

Here, K_{CT} is the complexation constant, C_A^0 and C_D^0 are the initial acceptor and donor concentrations, and C_{AD} is the CTC concentration at equilibrium. Our measurements of CTC absorption are directly related to C_{AD} by Beer's Law, $Abs = \varepsilon C_{AD} l$, in which Abs is the concentration-dependent absorbance (or optical density, OD) and ε is the extinction coefficient of the CTC at a specific wavelength (l is the sample pathlength, which was 1 cm in our measurements). These relationships can be used to derive a (nonlinear) relationship between sample absorbance, formation constant, and the initial donor and acceptor concentrations[42]:

$$Abs = \frac{\varepsilon}{2}\left[\left(C_A^0 + C_D^0 + \frac{1}{K_{CT}}\right) - \sqrt{\left(C_A^0 + C_D^0 + \frac{1}{K_{CT}}\right)^2 - 4C_A^0 C_D^0}\right] \quad (2)$$

A standard approach for determining formation constants for CTCs is to apply the Benesi-Hildebrand method[43] (or related linear-fitting methods[44-47]) to measurements of CTC absorption as a function of either the donor or acceptor concentration. Benesi-Hildebrand analysis relies on a large excess of the acceptor or donor concentration, respectively, which results in a linearized expression from Equation 2 that relates CTC absorption, donor/acceptor concentration, and ε and K_{CT}. This has been applied in several studies involving weak donor-acceptor CTCs but has been subject to debate regarding inaccuracy in determining formation constants.[42, 48-52] An alternative approach is to use nonlinear regression to fit data directly to Equation 2.[53-55] Although this approach does not place strict limits on the concentrations of individual species that should be used

or make any fitting approximations, the following inequalities have been proposed to improve reliability for determinations of K_{CT} and ε, assuming $C_D^0 > C_A^0$:

$$0.1C_A^0 < C_{AD} < 0.9C_A^0 \text{ or } 0.1/K < C_D^0 < 0.9/K \quad (3)$$

$$0.2 \leq s \leq 0.8 \qquad s = C_{AD}/C_A^0 \quad (4)$$

where *s* is the saturation fraction for the concentration of the complex with respect to the initial concentration of the limiting reagent and where it is suggested to analyze at least 75% of the saturation curve.[45, 56] In essence, these recommendations ensure that there is curvature in a plot of Abs vs C_D^0, which makes it easier to simultaneously determine K_{CT} and ε with greater accuracy. Finally, for improved accuracy in determining K_{CT} and ε, it has been reported that 10-15 data points for a fit of *Abs* vs concentration should be included (which can be over a broad range of donor or acceptor concentrations).[42]

The formation constant for the CT complex in DCM and its extinction coefficient at 750 nm were determined by fitting the absorbance data plotted in Figure 2a to Equation 2 with a nonlinear least-squares regression using Matlab's "fitnlm" command. The resulting fit curve is plotted with experimental data in Figure 2b. Best-fit values of 4.8 ± 0.6 × 10^4 M^{-1} and 2.42 ± 0.04 × 10^4 M^{-1} cm^{-1} were obtained for K_{CT} and ε, respectively. The large value for the formation constant was expected given the combination of strong electron-donating and accepting species and the relatively high dielectric constant of the solvent medium that is expected to stabilize the charge-transfer complex. We also note that we previously estimated the extinction coefficients for $F_4TCNQ^{\cdot -}$ and $MPDA^+$ in dichloroethane at 750 nm to be 1.9 × 10^4 and 9.5 × 10^3 M^{-1} cm^{-1}, respectively, using controlled potential electrolysis.[16] The sum of these values is in reasonable agreement with the fit value for ε (2.48 ± 0.02 × 10^4 vs 2.85 × 10^4) [Note: to determine the

extinction coefficient in our previous work, the CTC concentration was estimated from the initial donor and acceptor concentrations in CPE measurements.[16]]

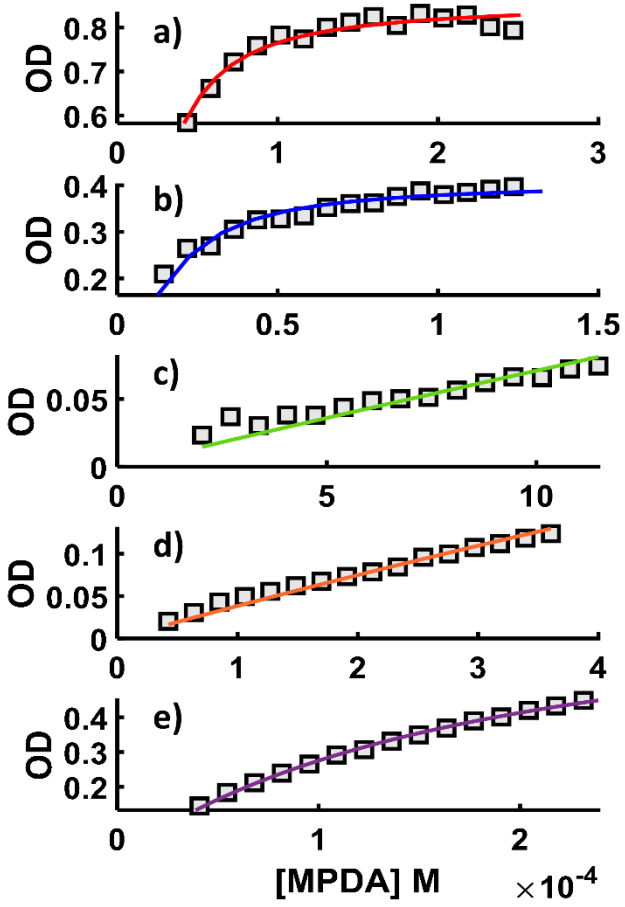

Figure 3. Absorption with donor concentration with fits to Equation 2 for CTCs in (a) 1,2-dichloroethane, (b) 1,2-dichlorobenzene, (c) ethyl acetate, (d) chlorobenzene, and (e) chloroform. Best-fit parameters are listed in Table 1.

To investigate the impact of local (solvent) environment on complex formation, CTCs were prepared in a collection of solvents with a range of permittivity and polarity; complexation constants were determined with the same experimental procedures and analyses presented above. We anticipated a decrease in K_{CT} with decrease in solvent dielectric constant (i.e. solvents of effectively lower permittivity being less suited to stabilize the charged vs. neutral donor-acceptor

pair), with the goal of determining how low the solvent permittivity can be and still stabilize integer charge transfer between the donor-acceptor pair. Figure 3 plots the absorption at 750 nm with donor concentration for integer CTCs in 1,2-dichloroethane (a), 1,2-dichlorobenzene (b), chlorobenzene (d), and chloroform (e). Curves of best-fit to Equation 2 are overlaid as colored lines; fitting parameters for this series of solvents are listed in Table 1. Tabulated concentrations and optical densities are provided in Tables S2-S5; fits for each data set are presented independently in Figures S3-S6. Within the standard error of the best-determined values for K_{CT}, a decrease in the CTC formation constant is observed when decreasing solvent permittivity in the chlorinated series from DCE to CB. The formation constant in chloroform deviates from this trend and will be discussed in further detail below in terms of enthalpic and entropic contributions to CTC stabilization.

Table 1. Best-fit K_{CT} and ε (extinction coefficient) obtained for CTCs in solvents of various permittivity (dielectric constant). For the cases of ethyl acetate and chlorobenzene, the value of ε was allowed to vary or was bound to specified values listed in the brackets to obtain corresponding values for K_{CT}.

Solvent	Dielectric Constant	K_{CT} (M^{-1})	ε (M^{-1} cm^{-1})
1,2-Dichloroethane	10.36	$1.2 \pm 0.1 \times 10^5$	$2.48 \pm 0.02 \times 10^4$
1,2-Dichlorobenzene	9.93	$1.5 \pm 0.2 \times 10^5$	$2.06 \pm 0.04 \times 10^4$
Dichloromethane	8.93	$4.8 \pm 0.6 \times 10^4$	$2.42 \pm 0.04 \times 10^4$
Ethyl Acetate	6.02	$1.0 \pm 0.3 \times 10^3$ [48.3, 25.0]	$8.1 \pm 1.2 \times 10^2$ [9×10^3, 1.7×10^4]
Chlorobenzene	5.62	$1.5 \pm 0.2 \times 10^3$ [3.4×10^2, 2.8×10^2]	$5.9 \pm 0.6 \times 10^3$ [2×10^4, 2.4×10^4]
Chloroform	4.81	$6.5 \pm 0.3 \times 10^3$	$1.96 \pm 0.05 \times 10^4$

We also examined complexation in a non-chlorinated solvent, ethyl acetate (ε = 6.02). As observed for solutions with chlorobenzene, only weak complexation was observed in these solutions compared to solutions made with solvents of higher permittivity. Notably, weak signatures of F_4TCNQ anion were observed in absence of the donor (UV-Vis spectrum presented in Figure S7); similar behavior has been noted for TCNQ dissolved in other solvents and could be

the result of complexation with solvent or a chemical stabilizer (or contaminant) present in small concentrations.[57] We estimated the concentration of anion present in the stock solution at 2×10^{-6} M using the extinction of the anion in dichloroethane; importantly, this concentration is negligible compared to the starting concentration of acceptor (3.4×10^{-4} M), and should not affect the donor-acceptor complexation equilibrium in this solvent. However, the appearance of the anion in absence of donor does obscure signatures of the CTC absorption at 750 nm given that the equilibrium is considerably weaker in this solvent. Consequently, we analyzed the donor-concentration-dependent absorption at 1000 nm for CTCs in ethyl acetate to determine K_{CT} and ε, as this wavelength is selective for absorption of the MPDA radical cation and any change in absorption here should be associated only with the MPDA cation formed as part of the charge-transfer complex. The associated concentration-dependent trace and nonlinear fit are shown in Figure 3(c) and the fit parameters are presented in Table 1. Tabulated concentrations and optical densities are provided in Tables S6.

We note that for 1,2-dichloroethane, 1,2-dichlorobenzene, dichloromethane, and chloroform, the fitted extinction coefficient ε ranges between 2 - 2.4×10^4 $M^{-1}cm^{-1}$, consistent with the magnitude estimated from our prior work. The value obtained for chlorobenzene by least-squared nonlinear fit is unexpectedly much lower (~ 6×10^3 M^{-1} cm^{-1}) than the value obtained in all other solvents, and is most likely unphysical, as we do not expect that the ion's absorptivity should be so sensitive to solvent. We therefore performed similar nonlinear fits of the formation constant with ε constrained between 2×10^4 $M^{-1}cm^{-1}$ and 2.4×10^4 $M^{-1}cm^{-1}$ to provide a bracketed estimate of K_{CT}. The resulting values are reported in Table 1 alongside results from fits in which the extinction coefficient and K_{CT} were simultaneously fit without constraints. Together, these results point to a formation constant below 10^3 in CB (and more realistically within the range of a

few hundred). We applied a similar approach with complex formation in ethyl acetate, but with ε bound at 9×10^3 $M^{-1}cm^{-1}$ or 1.7×10^4 $M^{-1}cm^{-1}$ based on an estimated extinction coefficient of 1.3×10^4 $M^{-1}cm^{-1}$ at 1000 nm from UV-Vis of electrochemically generated MPDA radical cation in DCE. This approach similarly results in very low values for the formation constant in this solvent (even below 10^2). Based on data for this full data set covering permittivity ranging ϵ~5-11, we observe an onset for highly favorable complexation at ϵ~8-9.

The local permittivity can be expected to impact the stability of donor-acceptor charge separation as follows: Within a dielectric continuum model, the absolute magnitude of the (negative) free energy associated with Coulombic charge-pair interaction will decrease with increasing permittivity due to charge screening; in contrast, the absolute magnitude of the (negative) solvation energy of an ionic species will increase with increasing permittivity, as predicted by the Born model.[58-59] These effects together are expected to impact the driving force for charge transfer, where it is assumed that permittivity has smaller impacts on the solvation energies of neutral reactants relative to charged products. We estimated the changes in solvation and ion-pair interaction energies assuming an ionic "radius" of 5 Å for each product ion and a comparable ion-pair separation; these factors alone predict a ~150 meV increase in the stability of the ion pair with ϵ~11 vs. ϵ~5. Notably, this is on the same order as the free energy gap determined electrochemically in DCE[16] (ϵ~11) and would explain the precipitous drop in formation constant observed between these values of permittivity (i.e. the driving force diminishes appreciably as permittivity is decreased).

Thermodynamics of $MPDA^{\cdot+}$:$F_4TCNQ^{\cdot-}$ Complexation

The combined free-energy change associated with donor oxidation and acceptor reduction was computed for each solvent environment and was compared with the free-energy of

complexation obtained from the experimentally-determined value of K_{CT}. Both values are listed in Table 2. The same qualitative trend is observed in both experimental and computational results: free energy decreases with decrease in solvent dielectric. We have previously reported a change in sign in calculated free energy for charge transfer in toluene, consistent with our experimental observation that no CTCs are formed in toluene solutions.[16] We note that these computation-based estimations do not consider the Coulombic interaction between the charged species, nor do they account for enthalpies of specific solute-solvent interactions or entropy changes associated with changes in solvent-solute interactions. Nonetheless, both sets of values are consistent with the predicted permittivity dependence in solvent stabilization of charged products described above.

Table 2. Free energies for acceptor reduction and donor oxidation used to determine approximate free energy for CTC formation (ΔG_{CTC}) for comparison to experimentally determined values.

Solvent	$F_4TCNQ/F_4TCNQ^{\cdot -}$ (kcal/mol)[a]	$MPDA^{\cdot +}/MPDA$ (kcal/mol)[a]	ΔG_{CTC} Calculated (kcal/mol)[b]	ΔG_{CTC} Experimental (kcal/mol)[c,d]
1,2-Dichloroethane	-117.98	-104.96	-13.02	-6.84 ± 0.05
1,2-Dichlorobenzene	-117.88	-106.0	-11.88	-7.0 ± 0.1
Dichloromethane	-117.60	-106.48	-11.12	-6.30 ± 0.03
Ethyl Acetate	-116.42	-107.86	-8.55	-4.0 ± 0.2 (-2.07 ± 0.19)
Chlorobenzene	-116.32	-108.19	-8.13	-4.27 ± 0.16 (-3.35 ± 0.06)
Chloroform	-115.57	-109.13	-6.44	-5.1 ± 0.2
Toluene	-109.94	-113.99	4.05	-

[a] Calculated free energy of reduction for $X + e^- \rightarrow X^-$
[b] Difference of first two columns
[c] $\Delta G_{CTC} = -RT\ln(K_{CT})$
[d] Values in parentheses reflect the gap in ΔG_{CTC} values obtained when K_{CT} is determined with bracketed values for ε.

Temperature-dependent UV-Vis measurements were performed for CTC solutions in select solvents to assess enthalpic vs. entropic contributions to the free energy of complexation. Figure 4 plots the absorption at 750 nm for a series of CTC solutions in oDCB prepared at various donor concentrations over the range of 21 - 65 °C. A decrease in the curvature to the concentration dependence of absorbance is observed with increasing temperature in this range, which is consistent with an inverse relationship between K_{CT} and temperature. Fit parameters obtained from nonlinear fits to Equation 2 for each temperature are reported in Table 3 (donor and acceptor concentrations for each sample and optical densities of each sample at each temperature are presented in Table S7). We note that there is a slight decrease in the fitted extinction coefficient at 750 nm as temperature increases. Peak-normalized plots of spectra collected at each temperature for a common donor concentration do not exhibit signatures of spectral broadening with increasing temperature that could explain a decrease in ε at elevated temperature. Hence, these variations in ε may rather result from a small interdependence between K_{CT} and ε in the nonlinear fitting procedure.

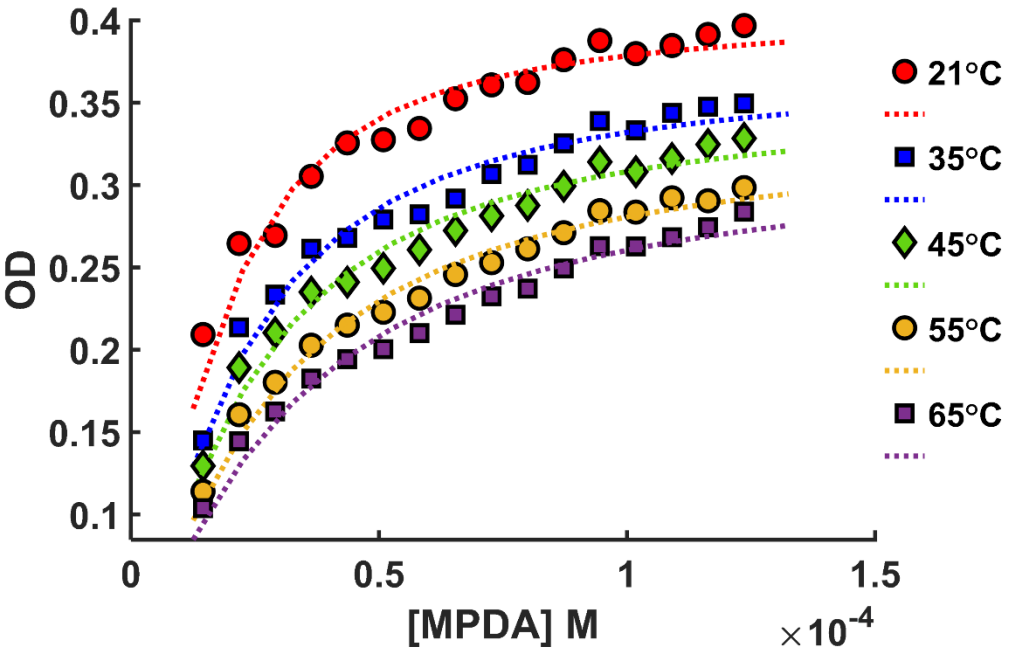

Figure 4. Temperature-dependent absorption at 750 nm for $MPDA^{\cdot+}$:$F_4TCNQ^{\cdot-}$CTCs dissolved in 1,2-dichlorobenzene prepared at various donor concentrations. Fits to Equation 2 are plotted as dashed lines.

Table 3. Temperature-dependent values of K_{CT} and ε for complexes in 1,2-Dichlorobenzene.

Temperature (K)	K_{CT} (M^{-1})	ε (cm^{-1} M^{-1})
294	$1.5 \pm 0.2 \times 10^5$	$2.06 \pm 0.04 \times 10^4$
308	$9.1 \pm 1.1 \times 10^4$	$1.89 \pm 0.04 \times 10^4$
318	$7.4 \pm 0.9 \times 10^4$	$1.80 \pm 0.04 \times 10^4$
328	$5.8 \pm 0.6 \times 10^4$	$1.70 \pm 0.03 \times 10^4$
338	$4.8 \pm 0.6 \times 10^4$	$1.63 \pm 0.05 \times 10^4$

Temperature-dependent measurements with solutions of the CTC in CB and $CHCl_3$ were also conducted to assess thermodynamic parameters associated with highly vs. weakly favorable complexation, as well as provide insight on the unexpectedly favorable complexation observed in $CHCl_3$. The concentration/absorbance data with fits to Equation 2 are presented in Figure S8 and S9 for chlorobenzene and chloroform solutions, respectively, at various temperatures; concentration/absorbance data is tabulated in Tables S8 and S10, with fitting parameters listed in

Tables S9 and S11, respectively. Temperature-dependent K_{CT} values obtained for solutions in each solvent were used to determine the enthalpy and entropy of complexation through linear fits to Equation 5:

$$ln(K_{CT}) = \frac{-\Delta H}{RT} + \frac{\Delta S}{R} \quad (5)$$

Figure 5 presents the fits to temperature-dependent values of K_{CT}. Values for enthalpies and entropies of complexation determined from these fits are listed in Table 4.

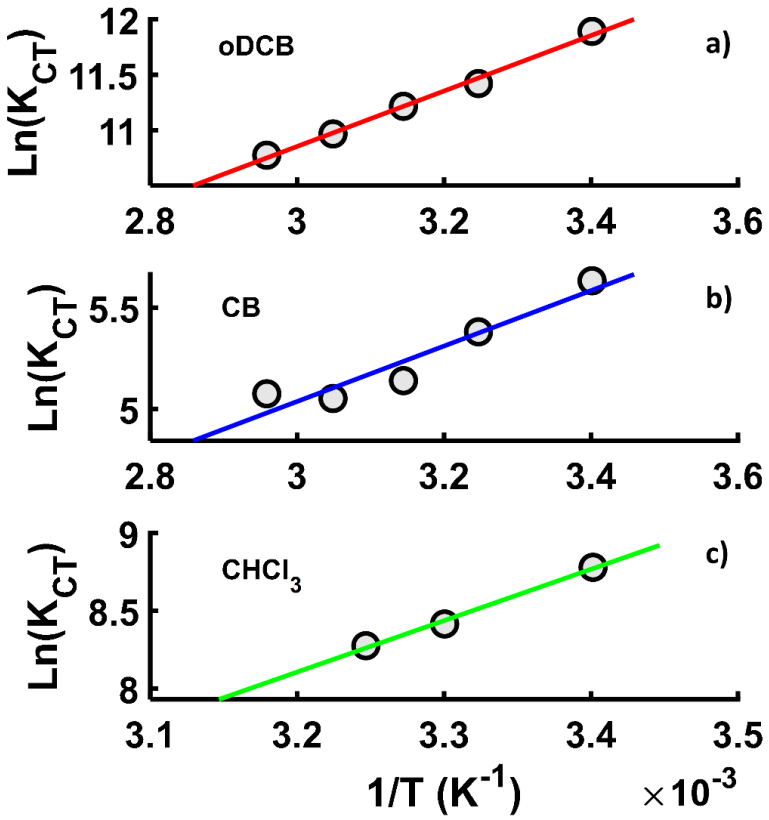

Figure 5. Temperature-dependence of K_{CT} for CTCs in (a) 1,2-dichlorobenzene, (b) chlorobenzene, (c) and chloroform. Enthalpies and entropies were determined from the best-fit line according to Equation 5. Best-fit parameters are listed in Table 4.

Table 4. Entropies and enthalpies obtained from temperature-dependent fits shown in Figure 5.

Solvent	Dielectric Constant	ΔH experimental (kcal mol^{-1})	ΔH calculated (kcal mol^{-1})	ΔS experimental (kcal mol^{-1} K^{-1})	ΔS calculated (kcal mol^{-1} K^{-1})
1,2-Dichlorobenzene	9.93	-4.97 ± 0.2	-11.80	0.0067 ± 0.0007	0.08
Chlorobenzene	5.62	-2.72 ± 0.5	-7.76	0.0018 ± 0.0016	0.37
Chloroform	4.81	-6.57 ± 0.5	-6.08	- 0.0049 ± 0.0017	0.36

For CTC formation in oDCB, where large complexation constants are observed, a negative ΔH and small positive ΔS were obtained, signifying that CTC formation is highly favorable and exothermic in the higher polarity solvents that can support charge separation. Similarly, in chlorobenzene, where complex formation is weakly favorable at room temperature, charge separation is observed to be exothermic but with much smaller values of ΔH and ΔS. The smaller enthalpy could be viewed as a weaker solvent stabilization of the charged products. Computed thermodynamic parameters are in qualitative accord with this observed behavior.

Chloroform is the interesting case where K_{CT} is high in a solvent environment with a relatively low permittivity. Here we observe formation of CTCs to be enthalpically favored, with a larger ΔH than determined for oDCB, but with a negative ΔS; this does not follow expectations from computations and signals that specific solvent-solute interactions support the formation of charge-separated pairs in these solutions. A possible explanation for this is weak hydrogen bonding,[60-61] which would result in increased solvent ordering around the charge pair complex compared to the neutral donor-acceptor ion pair and a resulting decrease in entropy upon complexation. Similarly the presence of local hydrogen bonding would result in stronger solvent-solute interaction, resulting in a greater enthalpic stabilization of charge-separated pairs.

Conclusion

We have characterized the influence of local (solvent) medium on the formation of charge transfer complexes between F_4TCNQ and the phenylene diamine donor MPDA. Equilibrium constants (K_{CT}) for formation in solvents covering a range of permittivity were obtained by nonlinear fit of the CTC absorption as a function of acceptor concentration (at a fixed F_4TCNQ concentration). Strongly favorable complexation ($K_{CT}>10^4$) occurs above a threshold permittivity in the range of 8-9; comparatively weak complexation ($K_{CT}<10^3$) is observed for permittivity below this threshold (with anomalously, strongly favored complexation in $CHCl_3$). This trend matches qualitatively with calculated oxidation-reduction energies for this donor-acceptor pair in each solvent represented as a polarizable continuum. CTC formation in solvents with permittivity ranging from 5 to 11 are observed to be both enthalpically and entropically favored. Given that the energy of ion-pair attraction decreases with increase in dielectric constant, this increase in driving force for charge-transfer with increasing permittivity must originate from an increased contribution from ion solvation, such as would be predicted by continuum solvation models (e.g. Born equation). Complexation in chloroform is anomalous, with the largest reported ΔH and a small negative ΔS. These findings indicate that specific, solvent-solute interactions contribute to stabilizing the charge transfer pair in this solvent.

Molecular charge doping has the potential to increase charge densities to improve the performance (conductivity, photoconductivity, etc.) of organic optoelectronics. The toolbox for controlling the extent of integer charge transfer has largely involved the selection of dopants with high electron affinity and by manipulating the microstructure of organic materials (with impacts on the electronic structure of the doped material and stability of charge-separated pairs as may be possible by increased charge delocalization). An additional approach for ensuring integer charge

separation is to tune permittivity (through chemical functionality) to support charge separation. This approach has been explored previously to enhance doping and charge separation efficiencies.[62-64] An important conclusion from our work is that only modest increases in permittivity are necessary to enhance the stability of ICT states associating with the chemical doping of hole-transporting materials with F_4TCNQ.

ASSOCIATED CONTENT

Supporting Information

Additional experimental results and data analyses, including concentration- and solvent-dependent absorption data for CTCs and analysis of solvent- and temperature-dependent complexation equilibria. This material is free of charge at the ACS publications website.

AUTHOR INFORMATION

Corresponding Author

Email: artbragg@jhu.edu

ORCID

Arthur E. Bragg: 0000-0002-3376-5494

Howard E. Katz: 0000-0002-3190-2475

ACKNOWLEDGEMENTS

This work was supported by the U.S. DOE grant DE-FG02-07ER46465.

References Cited

1. Goetz, K. P.; Vermeulen, D.; Payne, M. E.; Kloc, C.; McNeil, L. E.; Jurchescu, O. D., Charge-Transfer Complexes: New Perspectives on an Old Class of Compounds. *J. Mater. Chem. C* **2014**, *2*, 3065-3076.

2. Wang, W.; Luo, L. X.; Sheng, P.; Zhang, J.; Zhang, Q. C., Multifunctional Features of Organic Charge-Transfer Complexes: Advances and Perspectives. *Chem. Eur. J.* **2021**, *27*, 464-490.

3. Jacobs, I. E.; Moulé, A. J., Controlling Molecular Doping in Organic Semiconductors. *Adv. Funct. Mater.* **2017**, *29*, 1703063.

4. Lüssem, B.; Riede, M.; Leo, K., Doping of Organic Semiconductors. *Phys. Status Solidi A* **2013**, *210*, 9-43.

5. Tietze, M. L.; Benduhn, J.; Pahner, P.; Nell, B.; Schwarze, M.; Kleeman, H.; Krammer, M.; Zojer, K.; Vandewal, K.; Leo, K., Elementary Steps in Electrical Doping of Organic Semiconductors. *Nat. Commun.* **2018**, *9*, 1182.

6. Mulliken, R. S., Molecular Compounds and Their Spectra .2. *J. Am. Chem. Soc.* **1952**, *74*, 811-824.

7. Mulliken, R. S., Molecular Compounds and Their Spectra .3. The Interaction of Electron Donors and Acceptors. *J. Phys. Chem.* **1952**, *56*, 801-822.

8. Zhang, J.; Xu, W.; Sheng, P.; Zhao, G. Y.; Zhu, D. B., Organic Donor-Acceptor Complexes as Novel Organic Semiconductors. *Acc. Chem. Res.* **2017**, *50*, 1654-1662.

9. Méndez, H.; Heimel, G.; Opitz, A.; Sauer, K.; Barkowski, P.; Oehzelt, M.; Soeda, J.; Okamoto, T.; Takeya, J.; Arlin, J.-B., et al., Doping of Organic Semiconductors: Impact of Dopant Strength and Electronic Coupling. *Angew. Chem. Int. Ed.* **2013**, *52*, 7751-7755.

10. Stanfield, D. A.; Wu, Y.; Tolbert, S. H.; Schwartz, B. J., Controlling the Formation of Charge Transfer Complexes in Chemically Doped Semiconducting Polymers. *Chem. Mater.* **2021**, *33*, 2343-2356.

11. Aubry, T. J.; Axtell, J. C.; Basile, V. M.; Winchell, K. J.; Lindemuth, J. R.; Porter, T. M.; Liu, J. Y.; Alexandrova, A. N.; Kubiak, C. P.; Tolbert, S. H., et al., Dodecaborane-Based Dopants Designed to Shield Anion Electrostatics Lead to Increased Carrier Mobility in a Doped Conjugated Polymer. *Adv. Mater.* **2019**, *31*, 1805647.

12. Scholes, D. T.; Hawks, S. A.; Yee, P. Y.; Wu, H.; Lindemuth, J. R.; Tolbert, S. H.; Schwartz, B. J., Overcoming Film Quality Issues for Conjugated Polymers Doped with F4tcnq by Solution Sequential Processing: Hall Effect, Structural, and Optical Measurements. *J. Phys. Chem. Lett.* **2015**, *6*, 4786-4793.

13. Mendez, H.; Heimel, G.; Winkler, S.; Frisch, J.; Opitz, A.; Sauer, K.; Wegner, B.; Oehzelt, M.; Rothel, C.; Duhm, S., et al., Charge-Transfer Crystallites as Molecular Electrical Dopants. *Nat. Commun.* **2015**, *6*, 8560.

14. Pingel, P.; Neher, D., Comprehensive Picture of P-Type Doping of P3ht with the Molecular Acceptor F(4)Tcnq. *Phys. Rev. B* **2013**, *87*, 115209.

15. Salzmann, I.; Heimel, G., Toward a Comprehensive Understanding of Molecular Doping Organic Semiconductors (Review). *J. Electron. Spectrosc. Relat. Phenom.* **2015**, *204*, 208-222.

16. Barrett, B. J.; Saund, S. S.; Dziatko, R. A.; Clark-Winters, T. L.; Katz, H. E.; Bragg, A. E., Spectroscopic Studies of Charge-Transfer Character and Photoresponses of F(4)Tcnq-Based Donor-Acceptor Complexes. *J. Phys. Chem. C* **2020**, *124*, 9191-9202.

17. Ma, L.; Hu, P.; Jiang, H.; Kloc, C.; Sun, H.; Soci, C.; Voityuk, A. A.; Michel-Beyerle, M. E.; Gurzadyan, G. G., Single Photon Triggered Dianion Formation in Tcnq and F4tcnq Crystals. *Sci. Rep.* **2016**, *6*, 28510.

18. Kampar, E.; Neilands, O., Degree of Charge Transfer in Donor–Acceptor Systems of the П–П Type. *Russ. Chem. Rev.* **1986**, *55*, 334-342.

19. Meneghetti, M.; Pecile, C., Charge-Transfer Organic-Crystals - Molecular Vibrations and Spectroscopic Effects of Electron-Molecular Vibration Coupling of the Strong Electron-Acceptor Tcnqf4. *J. Chem. Phys.* **1986**, *84*, 4149-4162.

20. Watts, K. E.; Neelamraju, B.; Ratcliff, E. L.; Pemberton, J. E., Stability of Charge Transfer States in F4tcnq-Doped P3ht. *Chem. Mater.* **2019**, *31*, 6986-6994.

21. Neelamraju, B.; Watts, K. E.; Pemberton, J. E.; Ratcliff, E. L., Correlation of Coexistent Charge Transfer States in F4tcnq-Doped P3ht with Microstructure. *J. Phys. Chem. Lett.* **2018**, *9*, 6871-6877.

22. Theurer, C. P.; Richter, M.; Rana, D.; Duva, G.; Lepple, D.; Hinderhofer, A.; Schreiber, F.; Tegeder, P.; Broch, K., Coexistence of Ion Pairs and Charge-Transfer Complexes and Their Impact on Pentacene Singlet Fission. *J. Phys. Chem. C* **2021**, *125*, 23952-23959.

23. Cui, M. K.; Rui, H. S.; Wu, X. M.; Sun, Z.; Qu, W. X.; Qin, W. J.; Yin, S. G., Coexistent Integer Charge Transfer and Charge Transfer Complex in F4-Tcnq-Doped Ptaa for Efficient Flexible Organic Light-Emitting Diodes. *J. Phys. Chem. Lett.* **2021**, *12*, 8533-8540.

24. Salzmann, I.; Heimel, G.; Oehzelt, M.; Winkler, S.; Koch, N., Molecular Electrical Doping of Organic Semiconductors: Fundamental Mechanisms and Emerging Dopant Design Rules. *Acc. Chem. Res.* **2016**, *49*, 370-378.

25. Jiang, H.; Hu, P.; Ye, J.; Zhang, K. K. K.; Long, Y.; Hu, W. P.; Kloc, C., Tuning of the Degree of Charge Transfer and the Electronic Properties in Organic Binary Compounds by Crystal Engineering: A Perspective. *J. Mater. Chem. C* **2018**, *6*, 1884-1902.

26. Lee, I.; Rolston, N.; Brunner, P.-L.; Dauskardt, R. H., Hole-Transport Layer Molecular Weight and Doping Effects on Perovskite Solar Cell Efficiency and Mechanical Behavior. *ACS Appl. Mater. Interfaces* **2019**, *11*, 23757-23764.

27. Zhang, W.; Smith, J.; Hamilton, R.; Heeney, M.; Kirkpatrick, J.; Song, K.; Watkins, S. E.; Anthopoulos, T.; McCulloch, I., Systematic Improvement in Charge Carrier Mobility of Air Stable Triarylamine Copolymers. *J. Am. Chem. Soc.* **2009**, *131*, 10814-10815.

28. Hernandez-Verdugo, E.; Sancho-Garcia, J. C.; San-Fabian, E., The Application of Td-Dft to Excited States of a Family of Tpd Molecules Interesting for Optoelectronic Use. *Theor. Chem. Acc.* **2017**, *136*, 77.

29. Shirota, Y.; Kageyama, H., Charge Carrier Transporting Molecular Materials and Their Applications in Devices. *Chem. Rev.* **2007**, *107*, 953-1010.

30. El-ghandour, A.; Hameed, M. F. O.; Awed, A. S.; Obayya, S. S. A., Optical and Electrical Properties of Nanostructured N,N'-Diphenyl-N,N'-Di-P-Tolylbenzene-1,4-Diamine Organic Thin Films. *Appl. Phys. A* **2018**, *124*, 543.

31. Friend, R. H.; Gymer, R. W.; Holmes, A. B.; Burroughes, J. H.; Marks, R. N.; Taliani, C.; Bradley, D. D. C.; Dos Santos, D. A.; Bredas, J. L.; Logdlund, M., et al., Electroluminescence in Conjugated Polymers. *Nature* **1999**, *397*, 121-128.

32. Gao, W. Z.; Wang, S. R.; Xiao, Y.; Li, X. G., Study on Synthesis and Properties of Novel Luminescent Hole Transporting Materials Based on N,N '-Di(P-Tolyl)-N,N '-Diphenyl-1,1 '-Biphenyl-4,4 '-Diamine Core. *Dyes Pigm.* **2013**, *97*, 92-99.

33. Thelakkat, M.; Fink, R.; Haubner, F.; Schmidt, H. W., Synthesis and Properties of Novel Hole Transport Materials for Electroluminescent Devices. *Macromol. Symp.* **1998**, *125*, 157-164.

34. Neese, F.; Wennmohs, F.; Becker, U.; Riplinger, C., The Orca Quantum Chemistry Program Package. *J. Chem. Phys.* **2020**, *152*, 224108.

35. Neese, F., Software Update: The Orca Program System, Version 4.0. *Wiley Interdiscip. Rev. Comput. Mol. Sci.* **2018**, *8*, e1327.

36. Weigend, F.; Ahlrichs, R., Balanced Basis Sets of Split Valence, Triple Zeta Valence and Quadruple Zeta Valence Quality for H to Rn: Design and Assessment of Accuracy. *Phys. Chem. Chem. Phys.* **2005**, *7*, 3297-3305.

37. Schäfer, A.; Horn, H.; Ahlrichs, R., Fully Optimized Contracted Gaussian Basis Sets for Atoms Li to Kr. *J. Chem. Phys.* **1992**, *97*, 2571-2577.

38. Weigend, F., Accurate Coulomb-Fitting Basis Sets for H to Rn. *Phys. Chem. Chem. Phys.* **2006**, *8*, 1057-1065.

39. Job, P., Studies on the Formation of Complex Minerals in Solution and on Their Stability. *Ann. Chim. France* **1928**, *9*, 113-203.

40. Gil, V. M. S.; Oliveira, N. C., On the Use of the Method of Continuous Variations. *J. Chem. Educ.* **1990**, *67*, 473.

41. Olson, E. J.; Bühlmann, P., Getting More out of a Job Plot: Determination of Reactant to Product Stoichiometry in Cases of Displacement Reactions and N:N Complex Formation. *J. Org. Chem.* **2011**, *76*, 8406-8412.

42. Grebenyuk, S. A.; Perepichka, I. F.; Popov, A. F., Evaluation of the Parameters of 1 : 1 Charge Transfer Complexes from Spectrophotometric Data by Non-Linear Numerical Method. *Spectrochim. Acta A* **2002**, *58*, 2913-2923.

43. Benesi, H. A.; Hildebrand, J. H., A Spectrophotometric Investigation of the Interaction of Iodine with Aromatic Hydrocarbons. *J. Am. Chem. Soc.* **1949**, *71*, 2703-2707.

44. Scott, R. L., Some Comments on the Benesi-Hildebrand Equation. *Recl. Trav. Chim. Pays-Bas* **1956**, *75*, 787-789.

45. Deranleau, D. A., Theory of Measurement of Weak Molecular Complexes .I. General Considerations. *J. Am. Chem. Soc.* **1969**, *91*, 4044-4069.

46. Foster, R.; Hammick, D. L.; Wardley, A. A., Interaction of Polynitro-Compounds with Aromatic Hydrocarbons and Bases .11. A New Method for Determining the Association Constants for Certain Interactions between Nitro-Compounds and Bases in Solution. *J. Chem. Soc.* **1953**, 3817-3820.

47. Scatchard, G., The Attractions of Proteins for Small Molecules and Ions. *Ann. N.Y. Acad. Sci.* **1949**, *51*, 660-672.

48. McKim, W. D.; Ray, J.; Arnold, B. R., Analysis of the Association Constants for Charge-Transfer Complex Formation. *J. Mol. Struct.* **2013**, *1033*, 131-136.

49. Arnold, B. R.; Euler, A.; Fields, K.; Zaini, R. Y., Association Constants for 1,2,4,5-Tetracyanobenzene and Tetracyanoethylene Charge-Transfer Complexes with Methyl-Substituted Benzenes Revisited. *J. Phys. Org. Chem.* **2000**, *13*, 729-734.

50. Baniyaghoob, S.; Najafpour, M. M.; Boghaei, D. M., Charge-Transfer Complexes of 4-Nitrocatechol with Some Amino Alcohols. *Spectrochim. Acta A* **2010**, *75*, 970-977.

51. Jalilov, A. S.; Lu, J. J.; Kochi, J. K., Charge-Transfer Complex Formations of Tetracyanoquinone (Cyanil) and Aromatic Electron Donors. *J. Phys. Org. Chem.* **2016**, *29*, 35-41.

52. Varukolu, M.; Palnati, M.; Nampally, V.; Gangadhari, S.; Vadluri, M.; Tigulla, P., New Charge Transfer Complex between 4-Dimethylaminopyridine and Ddq: Synthesis, Spectroscopic Characterization, DNA Binding Analysis, and Density Functional Theory (Dft)/Time-Dependent Dft/Natural Transition Orbital Studies. *Acs Omega* **2022**, *7*, 810-822.

53. Perepichka, I. F.; Kuz'mina, L. G.; Perepichka, D. F.; Bryce, M. R.; Goldenberg, L. M.; Popov, A. F.; Howard, J. A. K., Electron Acceptors of the Fluorene Series. 7.1 2,7-Dicyano-4,5-

Dinitro-9-X-Fluorenes: Synthesis, Cyclic Voltammetry, Charge Transfer Complexation with N-Propylcarbazole in Solution, and X-Ray Crystal Structures of Two Tetrathiafulvalene Complexes. *J. Org. Chem.* **1998**, *63*, 6484-6493.

54. Perepichka, I. F.; Popov, A. F.; Orekhova, T. V.; Bryce, M. R.; Andrievskii, A. M.; Batsanov, A. S.; Howard, J. A. K.; Sokolov, N. I., Electron Acceptors of the Fluorene Series. 10.1 Novel Acceptors Containing Butylsulfanyl, Butylsulfinyl, and Butylsulfonyl Substituents: Synthesis, Cyclic Voltammetry, Charge-Transfer Complexation with Anthracene in Solution, and X-Ray Crystal Structures of Two Tetrathiafulvalene Complexes. *J. Org. Chem.* **2000**, *65*, 3053-3063.

55. D. Mysyk, D.; F. Perepichka, I.; I. Sokolov, N., Electron Acceptors of the Fluorene Series. Part 6.1 Synthesis of 4,5-Dinitro-9-X-Fluorene-2,7-Disulfonic Acid Derivatives, Their Charge Transfer Complexes with Anthracene and Sensitization of Photoconductivity of Poly-N-(2,3-Epoxypropyl)Carbazole. *J. Chem. Soc., Perkin trans.* **1997**, 537-546.

56. Person, W. B., A Criterion for Reliability of Formation Constants of Weak Complexes. *J. Am. Chem. Soc.* **1965**, *87*, 167-170.

57. Ma, L. H., P.; Kloc, C.; Sun, H.; Michel-Beyerle, M. E.; Gurzadyan, G. G., Ultrafast Spectroscopic Characterization of 7,7,8,8-Tetracyanoquinodimethane (Tcnq) and Its Radical Anion (Tcnq−). *Chem. Phys. Lett.* **2014**, *609*, 11-14.

58. Born, M., Volumen Und Hydratationswärme Der Ionen. *Z. Phys.* **1920**, *1*, 45-48.

59. Duignan, T. T.; Zhao, X. S., The Born Model Can Accurately Describe Electrostatic Ion Solvation. *Phys. Chem. Chem. Phys.* **2020**, *22*, 25126-25135.

60. Allen, F. H.; Wood, P. A.; Galek, P. T. A., Role of Chloroform and Dichloromethane Solvent Molecules in Crystal Packing: An Interaction Propensity Study. *Acta Cryst.* **2013**, *B69*, 379-388.

61. Gordy, W., Spectroscopic Evidence of Hydrogen Bonds: Chloroform and Bromoform in Donor Solvents. *J. Chem. Phys.* **1939**, *7*, 163-166.

62. Schwarze, M.; Gaul, C.; Scholz, R.; Bussolotti, F.; Hofacker, A.; Schellhammer, K. S.; Nell, B.; Naab, B. D.; Bao, Z.; Spoltore, D., et al., Molecular Parameters Responsible for Thermally Activated Transport in Doped Organic Semiconductors. *Nat. Mater.* **2019**, *18*, 242-248.

63. Kiefer, D.; Giovannitti, A.; Sun, H.; Biskup, T.; Hofmann, A.; Koopmans, M.; Cendra, C.; Weber, S.; Anton Koster, L. J.; Olsson, E., et al., Enhanced N-Doping Efficiency of a Naphthalenediimide-Based Copolymer through Polar Side Chains for Organic Thermoelectrics. *ACS Energy Lett.* **2018**, *3*, 278-285.

64. Dissanayake, D. S.; Gunathilake, S. S.; Udamulle Gedara, C. M.; Du, J.; Yoo, S. H.; Lee, Y.; Wang, Q.; Gomez, E. D.; Biewer, M. C.; Stefan, M. C., Conductive Triethylene Glycol Monomethyl Ether Substituted Polythiophenes with High Stability in the Doped State. *J. Polym. Sci. A Polym. Chem* **2019**, *57*, 1079-1086.

Supporting Information

for

Permittivity Threshold and Thermodynamics of Integer Charge-Transfer Complexation for an Organic Donor-Acceptor Pair

Brandon J. Barrett†, Howard E. Katz‡, and Arthur E. Bragg†*
†Department of Chemistry, Johns Hopkins University, 3400 N. Charles St., Baltimore, MD 21218

‡Department of Material Science & Engineering, Johns Hopkins University, 3400 N. Charles St., Baltimore, MD 21218

Table of Contents:

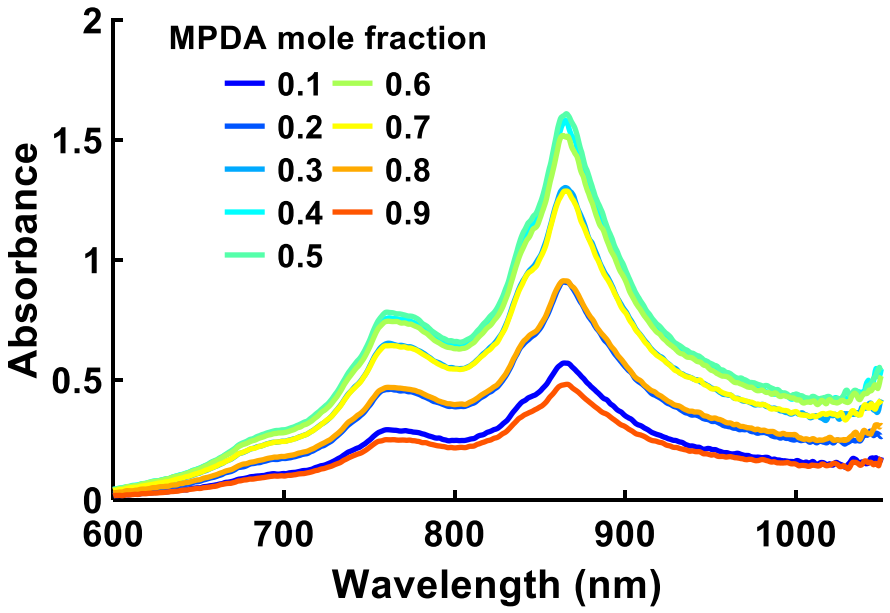

Figure S1. UV-Vis spectra of $MPDA^{\cdot+}$:$F_4TCNQ^{\cdot-}$ CTC in dichloromethane solutions prepared at various mole fractions of MPDA but constant donor+acceptor concentration (~$6x10^{-5}$ M).

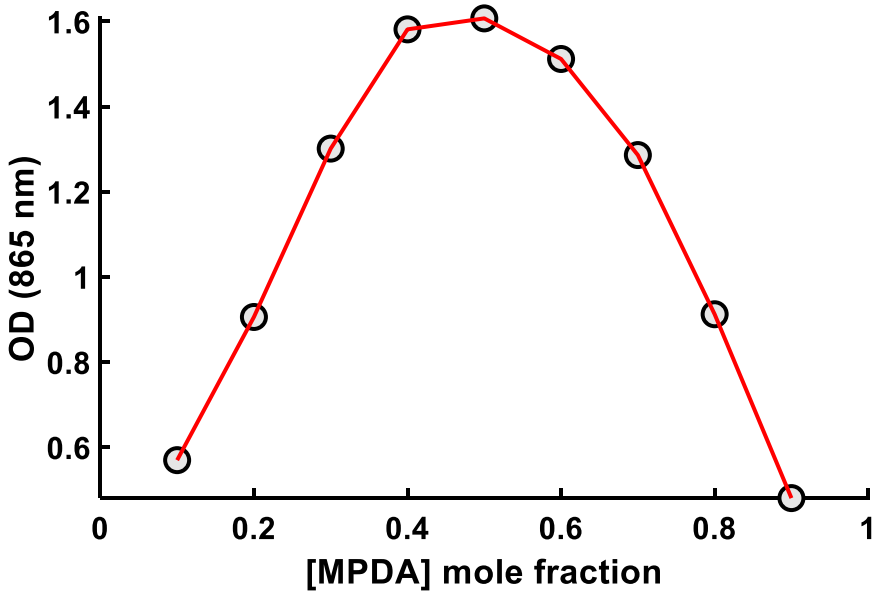

Figure S2. Jobs plot of $MPDA^{\cdot+}$:$F_4TCNQ^{\cdot-}$ CTC optical density (OD) at 865 nm taken from Figure S1. The peak at 0.5 mole fraction MPDA signifies a 1:1 donor:acceptor stoichiometry.

Table S1. Donor and acceptor concentrations used to prepare CTC solutions in dichloromethane with corresponding CTC absorbance at 750 nm. Measurements were made at room temperature (21 ºC).

[F_4TCNQ] (M)	**[MPDA] (M)**	**Absorbance (750 nm)**
4.71E-05	3.29E-05	0.524
4.71E-05	6.58E-05	0.663
4.71E-05	9.87E-05	0.884
4.71E-05	1.32E-04	0.925
4.71E-05	1.65E-04	0.990
4.71E-05	1.97E-04	0.986
4.71E-05	2.30E-04	1.014
4.71E-05	2.63E-04	1.030
4.71E-05	2.96E-04	1.057
4.71E-05	3.29E-04	1.078
4.71E-05	3.62E-04	1.066
4.71E-05	3.95E-04	1.098
4.71E-05	4.28E-04	1.083

Table S2. Donor and acceptor concentrations used to prepare CTC solutions in 1,2-dichloroethane with corresponding CTC absorbance at 750 nm. Measurements were collected at room temperature (21 ºC).

[F_4TCNQ] × 10^{-5} (M)	[MPDA] × 10^{-5} (M)	OD (750 nm)
3.47	4.36	0.583
3.47	5.81	0.662
3.47	7.26	0.722
3.47	8.72	0.759
3.47	10.2	0.783
3.47	11.6	0.774
3.47	13.1	0.801
3.47	14.5	0.812
3.47	16.0	0.825
3.47	17.4	0.805
3.47	18.9	0.832
3.47	20.3	0.821
3.47	21.8	0.829
3.47	23.2	0.802
3.47	24.7	0.794

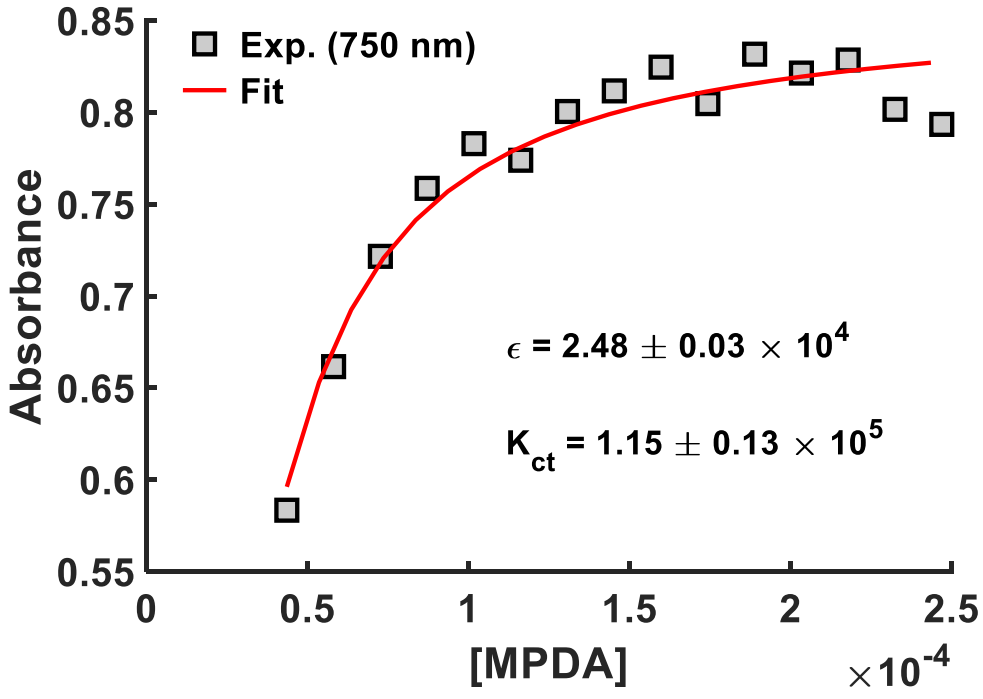

Figure S3. Plot of absorption at 750 nm (Table S2) vs. MPDA concentration for solutions of MPDA$^{\cdot+}$:F_4TCNQ$^{\cdot-}$ CTC in 1,2-dichloroethane. Experimental data points are shown as symbols; the nonlinear fit according to Equation 2 is plotted as a red line. Measurements were conducted at room temperature (21 ºC).

Table S3. Donor and acceptor concentrations used to prepare CTC solutions in 1,2-dichlorobenzene with corresponding CTC absorbance at 750 nm. Measurements were collected at room temperature (21 ºC).

[F_4TCNQ] × 10^{-5} (M)	[MPDA] × 10^{-5} (M)	OD (750 nm)
1.99	1.45	0.209
1.99	2.18	0.265
1.99	2.91	0.269
1.99	3.64	0.305
1.99	4.36	0.326
1.99	5.09	0.328
1.99	5.82	0.334
1.99	6.54	0.352
1.99	7.27	0.361
1.99	8.00	0.362
1.99	8.72	0.376
1.99	9.45	0.388
1.99	10.2	0.380
1.99	10.9	0.385
1.99	11.6	0.391
1.99	12.4	0.397

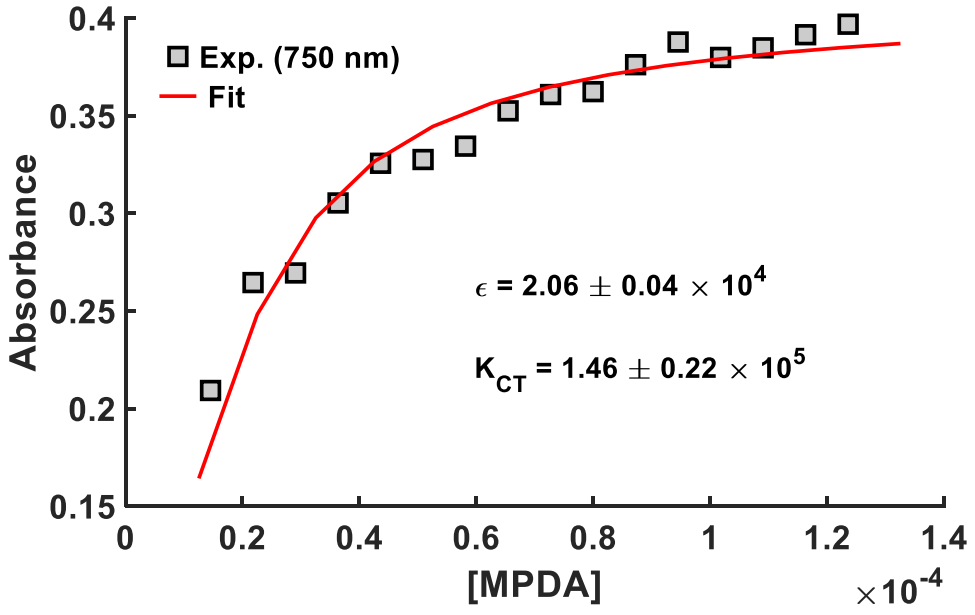

Figure S4. Plot of absorption at 750 nm (Table S3) vs. MPDA concentration for solutions of $MPDA^{\cdot+}$:$F_4TCNQ^{\cdot-}$ CTC in 1,2-dichlorobenzene. Experimental data points are shown as symbols; the nonlinear fit according to Equation 2 is plotted as a red line. Measurements were conducted at room temperature (21 ºC).

Table S4. Donor and acceptor concentrations used to prepare CTC solutions in chlorobenzene with corresponding CTC absorbance at 750 nm. Measurements collected at 21 ºC.

[F_4TCNQ] × 10^{-5} (M)	[MPDA] × 10^{-5} (M)	OD (750 nm)
5.98	4.24	0.020
5.98	6.36	0.031
5.98	8.48	0.043
5.98	10.6	0.050
5.98	12.7	0.056
5.98	14.8	0.062
5.98	17.0	0.068
5.98	19.1	0.073
5.98	21.2	0.078
5.98	23.3	0.084
5.98	25.5	0.096
5.98	27.6	0.100
5.98	29.7	0.107
5.98	31.8	0.112
5.98	33.9	0.118
5.98	36.1	0.123

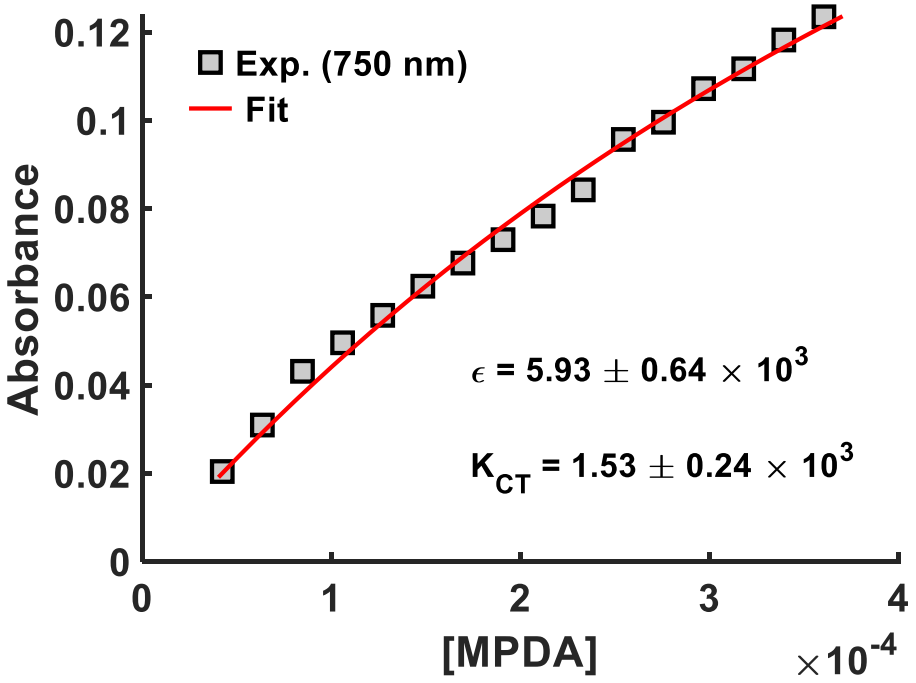

Figure S5. Plot of absorption at 750 nm (Table S4) vs. MPDA concentration for solutions of $MPDA^{\cdot+}$:$F_4TCNQ^{\cdot-}$ CTC in chlorobenzene. Experimental data points are shown as symbols; the nonlinear fit according to Equation 2 is plotted as a red line, with both K_{CT} and ϵ allowed to vary in fit. Measurements were conducted at room temperature (21 ºC).

Table S5. Donor and acceptor concentrations used to prepare CTC solutions in chloroform with corresponding CTC absorbance at 750 nm. Measurements collected at room temperature (21 ºC).

[F_4TCNQ] × 10^{-5} (M)	[MPDA] × 10^{-5} (M)	OD (750 nm)
2.94	3.06	0.145
2.94	4.09	0.184
2.94	5.11	0.212
2.94	6.13	0.239
2.94	7.15	0.265
2.94	8.17	0.292
2.94	9.19	0.307
2.94	10.2	0.331
2.94	11.2	0.349
2.94	12.3	0.369
2.94	13.3	0.390
2.94	14.3	0.401
2.94	15.3	0.420
2.94	16.3	0.433
2.94	17.4	0.448
2.94	30.6	0.145

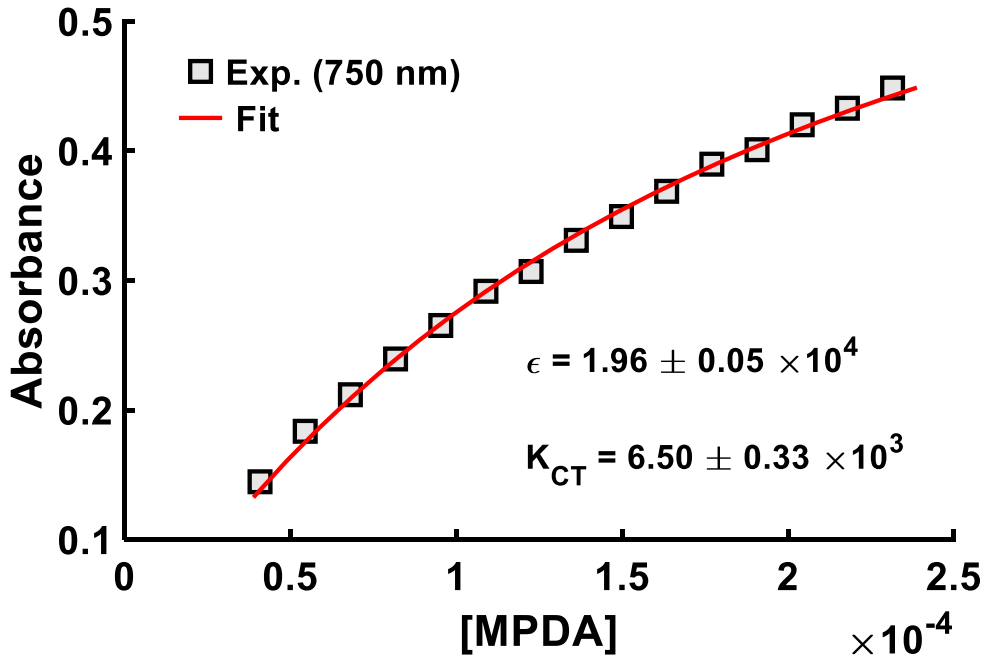

Figure S6. Plot of absorption at 750 nm (Table S5) vs. MPDA concentration for solutions of $MPDA^{\cdot+}$:$F_4TCNQ^{\cdot-}$ CTC in chloroform. Experimental data points are shown as symbols; the nonlinear fit according to Equation 2 is plotted as a red line, with both K_{CT} and ϵ allowed to vary in fit. Measurements were conducted at room temperature (21 ºC).

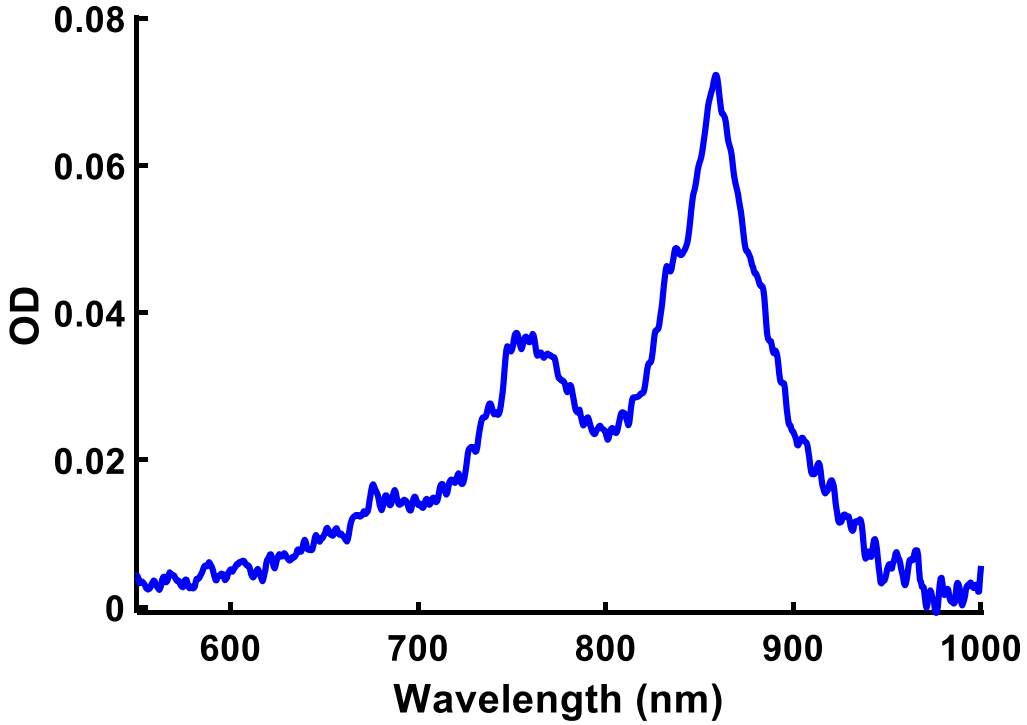

Figure S7. UV-Vis absorption spectrum of the F_4TCNQ stock solution used to prepare $MPDA^{\cdot+}$:$F_4TCNQ^{\cdot-}$ CTC solutions in ethyl acetate.

Table S6. Donor and acceptor concentrations used to prepare CTC solutions in ethyl acetate with corresponding absorbance at 1000 nm. Measurements collected at room temperature (21 ºC).

[F_4TCNQ] × 10^{-4} (M)	[MPDA] × 10^{-4} (M)	OD (1000 nm)
1.72	2.03	0.023
1.72	2.70	0.037
1.72	3.38	0.030
1.72	4.05	0.038
1.72	4.73	0.038
1.72	5.40	0.044
1.72	6.08	0.049
1.72	6.75	0.050
1.72	7.43	0.051
1.72	8.10	0.057
1.72	8.78	0.062
1.72	9.45	0.066
1.72	10.1	0.066
1.72	10.8	0.072
1.72	11.5	0.074

Table S7. Donor and acceptor concentrations used to prepare CTC solutions in 1,2-dichlorobenzene with corresponding absorbance at 750 nm. Measurements were conducted at listed temperatures.

[F_4TCNQ] × 10^{-5} (M)	[MPDA] × 10^{-5} (M)	OD 21°C	OD 35°C	OD 45°C	OD 55°C	OD 65°C
1.99	1.45	0.209	0.145	0.129	0.114	0.104
1.99	2.18	0.265	0.214	0.189	0.161	0.144
1.99	2.91	0.269	0.233	0.210	0.180	0.163
1.99	3.64	0.305	0.261	0.235	0.203	0.182
1.99	4.36	0.326	0.268	0.241	0.215	0.194
1.99	5.09	0.328	0.279	0.250	0.223	0.200
1.99	5.82	0.334	0.282	0.261	0.231	0.210
1.99	6.54	0.352	0.292	0.272	0.246	0.221
1.99	7.27	0.361	0.307	0.281	0.253	0.232
1.99	8.00	0.362	0.312	0.288	0.261	0.237
1.99	8.72	0.376	0.325	0.299	0.271	0.249
1.99	9.45	0.388	0.339	0.314	0.284	0.263
1.99	10.2	0.380	0.333	0.308	0.284	0.263
1.99	10.9	0.385	0.344	0.316	0.292	0.268
1.99	11.6	0.391	0.348	0.325	0.290	0.274
1.99	12.4	0.397	0.350	0.328	0.298	0.284

Table S8. Donor and acceptor concentrations used to prepare CTC solutions in chlorobenzene with corresponding absorbance at 750 nm. Measurements were conducted at listed temperatures.

[F_4TCNQ] × 10^{-5} (M)	[MPDA] × 10^{-5} (M)	OD 21°C	OD 35°C	OD 55°C	OD 65°C
5.98	4.24	0.020	0.021	0.017	0.017
5.98	6.36	0.031	0.030	0.020	0.022
5.98	8.48	0.043	0.034	0.026	0.028
5.98	10.6	0.050	0.039	0.028	0.032
5.98	12.7	0.056	0.045	0.031	0.038
5.98	14.8	0.062	0.048	0.038	0.039
5.98	17.0	0.068	0.052	0.039	0.043
5.98	19.1	0.073	0.059	0.045	0.047
5.98	21.2	0.078	0.064	0.048	0.047
5.98	23.3	0.084	0.066	0.052	0.052
5.98	25.5	0.096	0.074	0.056	0.056
5.98	27.6	0.100	0.081	0.059	0.063
5.98	29.7	0.107	0.086	0.061	0.058
5.98	31.8	0.112	0.089	0.062	0.062
5.98	33.9	0.118	0.092	0.068	0.068
5.98	36.1	0.123	0.098	0.069	0.070

Table S9. Temperature-dependent values of K_{CT} obtained for solutions of CTC in chlorobenzene by fitting data in Table S8 to Equation 2 of the main text (ε constrained to 2×10^4 at all temperatures).

Temperature (K)	K_{CT} (M^{-1})	ε (cm^{-1} M^{-1})
294	279.4	2.4×10^4
308	217.1	2.4×10^4
318	170.6	2.4×10^4
328	156.2	2.4×10^4
338	159.9	2.4×10^4

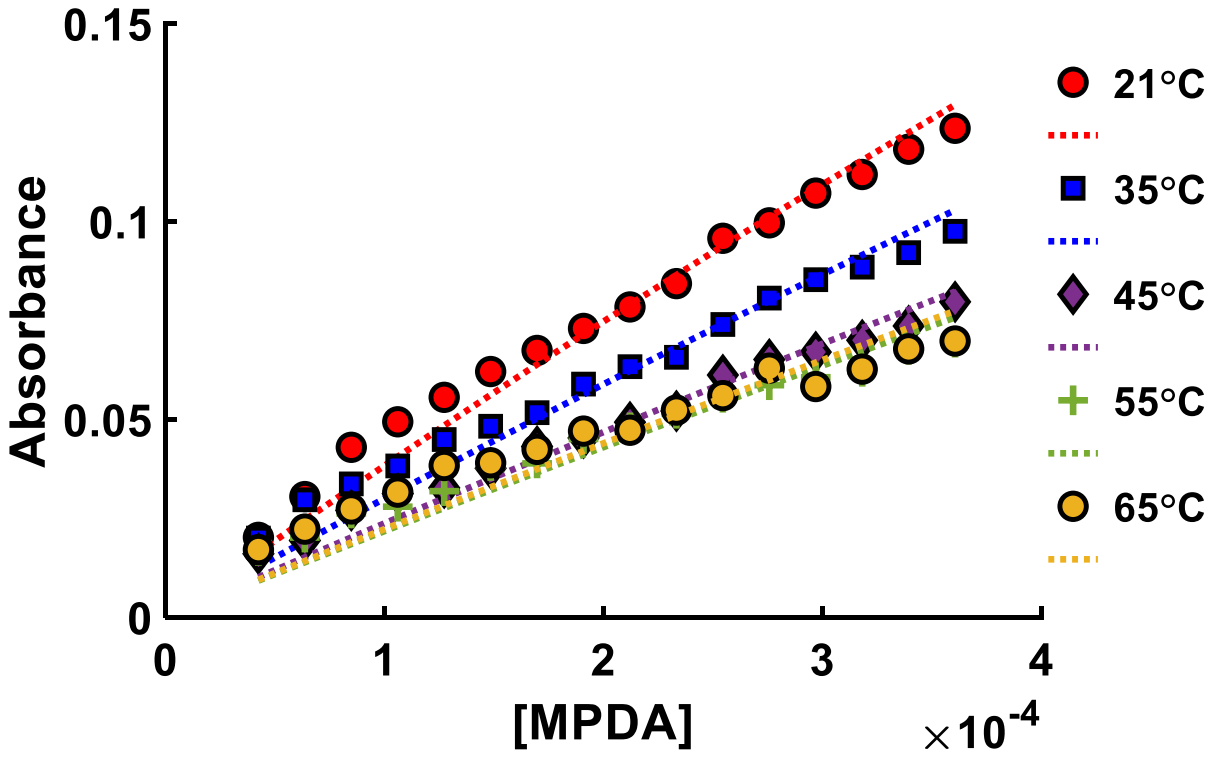

Figure S8. Temperature-dependent absorption at 750 nm vs. MPDA concentration for solutions of $MPDA^{\cdot+}$:$F_4TCNQ^{\cdot-}$ CTCs in chlorobenzene (data provided in Table 8) fit to Equation 2 of the main text with ε constrained to 2.4×10^4.

Table S10. Donor and acceptor concentrations used to prepare CTC solutions in chloroform with corresponding CTC absorbance at 750 nm. Measurements were conducted at the listed temperatures.

[F_4TCNQ] × 10^{-5} (M)	[MPDA] × 10^{-5} (M)	OD 21°C	OD 30°C	OD 35°C
2.94	3.06	0.145	0.101	0.088
2.94	4.09	0.184	0.129	0.110
2.94	5.11	0.212	0.151	0.130
2.94	6.13	0.239	0.174	0.148
2.94	7.15	0.265	0.195	0.169
2.94	8.17	0.292	0.216	0.188
2.94	9.19	0.307	0.232	0.200
2.94	10.2	0.331	0.248	0.216
2.94	11.2	0.349	0.266	0.233
2.94	12.3	0.369	0.282	0.245
2.94	13.3	0.390	0.307	0.260
2.94	14.3	0.401	0.308	0.273
2.94	15.3	0.420	0.322	0.281
2.94	16.3	0.433	0.337	0.299
2.94	17.4	0.448	0.348	0.311

Table S11. Temperature-dependent values of K_{CT} and ε obtained for CTC solutions dissolved in chloroform by fitting according to Equation 2 of the main text.

Temperature (K)	K_{CT} (M^{-1})	ε (cm^{-1} M^{-1})
294	8.66×10^3	2.61×10^4
303	6.02×10^3	2.40×10^4
308	5.23×10^3	2.28×10^4

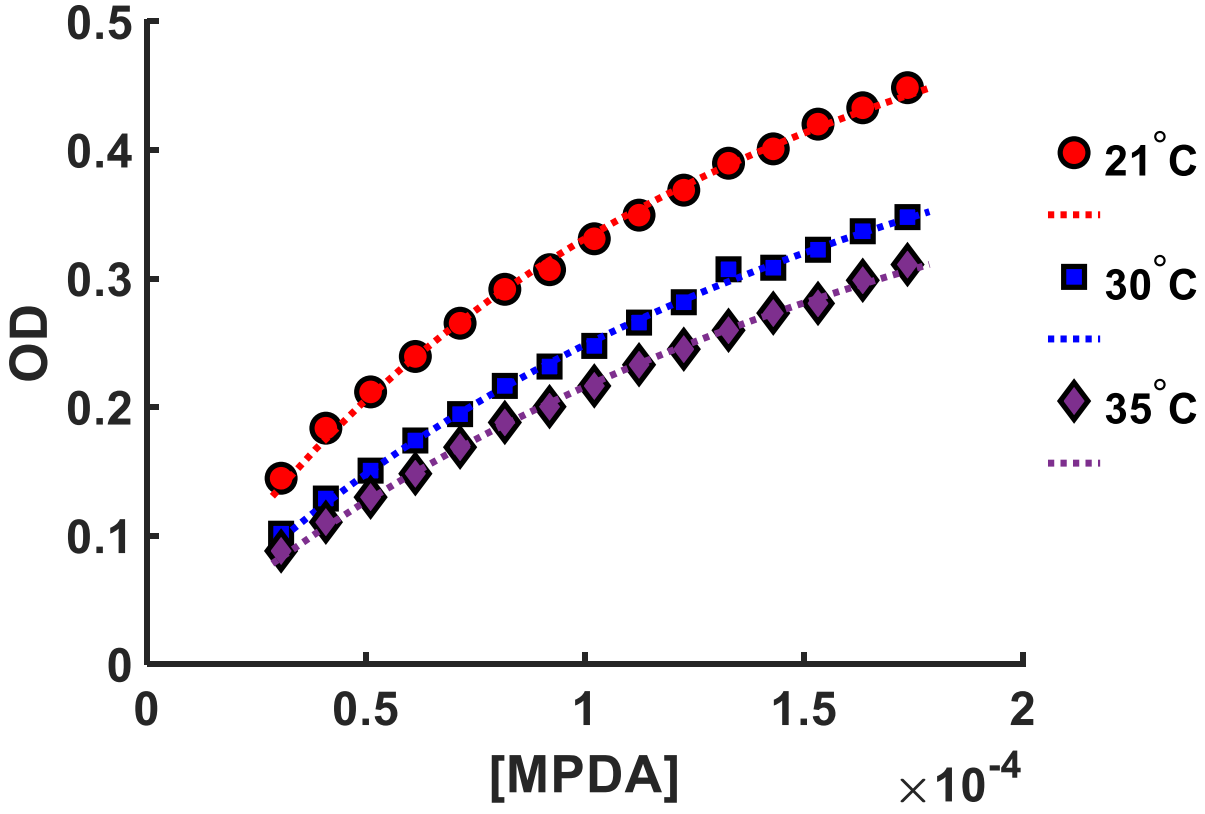

Figure S9. Temperature-dependent absorption at 750 nm vs. MPDA concentration for solutions of $MPDA^{\cdot+}$:$F_4TCNQ^{\cdot-}$ in chloroform (Table S10) fit with Equation 2 of the main text.